PNAS RESEARCH ARTICLE | COMPUTER SCIENCES

Communication by means of modulated Johnson noise

Zerina Kapetanovic[a,1], Miguel Morales[b], and Joshua R. Smith[a,c]

Edited by William Press, The University of Texas, Austin, TX; received January 24, 2022; accepted November 1, 2022

We present the design of a passive wireless communication method that does not rely on ambient or generated RF sources. Instead, the method modulates the Johnson (thermal) noise of a resistor to transmit information bits wirelessly. By selectively connecting or disconnecting a matched resistor to an antenna, the system can achieve data rates of up to 26 bps and distances of up to 7.3 m. This communication method operates at very low power, similar to that of an RFID tag, with the advantage of not requiring a preexisting RF signal to reflect.

wireless | communication | low-power | Johnson noise | backscatter

In passive wireless communication, an energy-constrained data transmitter sends information by modulating a radio frequency (RF) signal generated by an RF source that is not power constrained. Because the data transmitter does not have to generate an RF signal, the power necessary to send data is orders of magnitude less than in conventional RF communication. In modulated backscatter communication, a continuous wave RF carrier is generated by a dedicated device on the high-power side of the link, and the low-power side encodes data by selectively reflecting this RF signal (1). Ambient backscatter is another form of passive communication that makes use of preexisting, ambient RF signals such as those generated by broadcast TV or radio towers (2). While the low power of the data transmission side is attractive, both methods rely on a preexisting RF signal.

This paper introduces a form of passive wireless communication, Modulated Johnson Noise, in which the signal to be modulated is the Johnson noise in an unbiased (unpowered) resistor. This scheme retains the benefits of prior passive wireless communication schemes while eliminating the need for an external RF signal. This has the potential to reduce the overall energy consumption of the system, to allow stealthier and low-interference operation, and to allow operation in areas where no ambient RF signals are available.

Consider the frequency spectrum measurements shown in Fig. 1*A*, which shows the measured signal of a 50-Ω terminator and open circuit terminator connected to the input of a receiver. We can see that there is a clear difference between the two measurements, which can be exploited to enable wireless communication. By selectively connecting and disconnecting an impedance-matched 50-Ω resistor to an antenna, information bits can be wirelessly transmitted. For example, in Fig. 1*B*, we show the received signal of a data packet that was wirelessly transmitted by modulating Johnson noise. While this looks like a noisy signal, after performing demodulation, the data packet can be extracted as shown in Fig. 1*C*. While thermal noise communication has been proposed from a theoretical perspective (3), we present a system that enables wireless communication by modulating Johnson noise. In this paper, we discuss the design and experimental implementation of the system and evaluate the overall performance of the wireless communication scheme that relies on modulated Johnson noise. The contributions of the paper are summarized below:

- We introduce wireless communication by means of modulated Johnson noise, a wireless system that enables devices to communicate without reliance on generated or ambient RF signals.
- We present the designs and prototype of hardware that enables Johnson noise communication. Moreover, we demonstrate that the transmitter can be designed to be battery-free by performing solar energy harvesting and charging a supercapacitor rather than using a battery.
- We evaluate the performance of the wireless system in terms of achievable throughput and communication range. The performance evaluation shows that data rates of up to 26 bps can be achieved at distances of up to 7.3 m.

Significance

This paper presents experimental realization of an ultralow power wireless communication method that works by selectively connecting or disconnecting an impedance-matched resistor and an antenna. This modulates microwave frequency Johnson noise emitted by the antenna. The data transmission hardware is similar to that of an RFID tag, which communicates by reflecting RF signals; the crucial advantage of the present system is that it requires no preexisting RF signal. An interesting feature of the system is that all components of the system are at the same physical temperature, but it functions because they have different noise temperatures. It is also notable that the elimination of the RF carrier simplifies the system architecture and the reader hardware.

Author affiliations: [a]Department of Electrical and Computer Engineering, University of Washington, Seattle, WA 98195; [b]Department of Physics, University of Washington, Seattle, WA 98195; and [c]Department of Computer Science and Engineering, University of Washington, Seattle, WA 98195

Author contributions: Z.K. and J.R.S. designed research; Z.K. performed research; Z.K., M.M., and J.R.S. analyzed data; and Z.K. and J.R.S. wrote the paper.

Competing interest statement: A provisional patent has been filed on the subject matter with the USPTO.

This article is a PNAS Direct Submission.

[1]To whom correspondence may be addressed. Email: zerinak@uw.edu.

This article contains supporting information online at http://www.pnas.org/lookup/suppl/doi:10.1073/pnas.2201337119/-/DCSupplemental.

Published November 29, 2022.

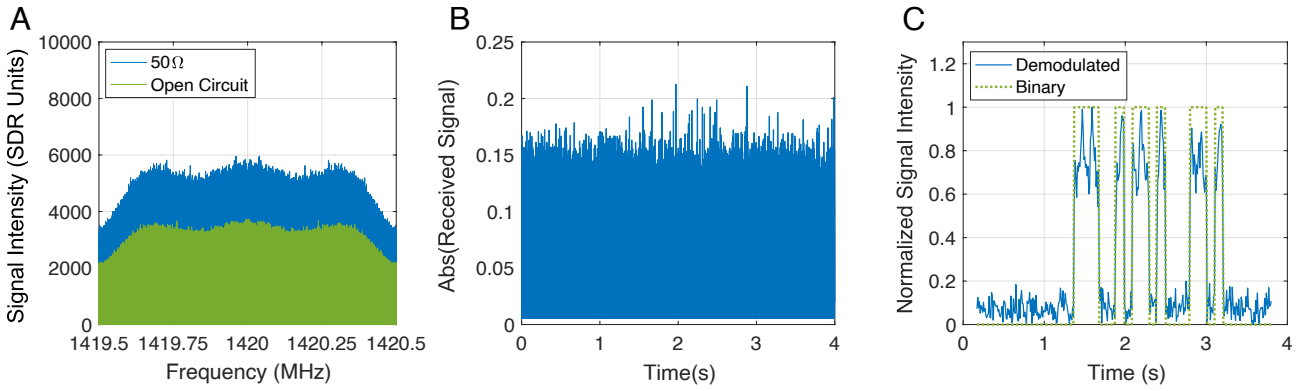

Fig. 1. Johnson noise communication. Wireless communication can be enabled by modulated Johnson noise. (*A*) shows the measured frequency spectrum at 1.42 GHz, which compares measurements when a 50-Ω load is connected to a receiver and an open circuit load. (*B*) shows what a received signal looks like when wirelessly transmitting a data packet by modulated Johnson noise, and (*C*) shows the received data packet after demodulation.

Overview of Johnson Noise

Johnson noise is caused by the thermal vibrations of charge carriers inside of an electrical conductor (e.g., resistor) and is characterized by its mean-squared voltage,

$$V_{\mathrm{n}}^2 = 4kTBRe(Z), \qquad [1]$$

where k is Boltzmann's constant, T is temperature, B is bandwidth, and $Re(Z)$ is the real part of the electrical conductor's impedance (4–6). A resistor with Johnson noise can be modeled as a Thevenin equivalent circuit that includes a noiseless resistor and a noise voltage generator with voltage given by Eq. **1**. With a matched load resistor connected, the maximum noise power provided by the noisy resistor is

$$P_{\mathrm{n}} = \frac{V_{\mathrm{n}}^2}{4R} = kTB, \qquad [2]$$

which is independent of resistance (7). The thermal noise power is a function of temperature and bandwidth. As an example, a resistor at room temperature (296 K) with a system bandwidth of 500 MHz would result in P_n = −86.9 dBm. We also note that Johnson noise is a white noise source and therefore independent of frequency (within the system's bandwidth). Moreover, Johnson noise has a Gaussian amplitude distribution.

Design and Implementation

We design and implement a transmitter (TX) and receiver (RX) to enable wireless communication by modulating Johnson noise. First, the transmitter requires an RF switch and a processing unit to control switching between an open or short circuit and resistor load connection shown in Fig. 2*A*. On the receive side, shown in Fig. 2*B*, two high gain, low noise amplifiers (LNA) amplify the very low-power signals being transmitted while maintaining a good signal-to-noise ratio. Between the two LNAs is a bandpass filter to prevent feedback oscillation. The entire system is designed to operate at 1.42 GHz with 50-Ω impedance. In Fig. 2 *C* and *D*, we show the prototype implementation of the transmitter and receiver. The transmitter uses an RF switch and switches between a 50-Ω RF terminator (with 50-Ω impedance) and an open circuit terminator, both of which are very well shielded (8). On the receive side, there are two LNAs with a combined gain of approximately 84 dB, a 50-MHz bandpass filter, and a software-defined radio (SDR) (9–11). We constructed pyramidal horn antennas for both the TX and RX sides. The antennas were characterized to have approximately 13.6 dBi of gain.

Data Encoding and Modulation. Since the transmitter is switching between two states, data can be modulated by performing ON–OFF keying. A 0 bit is transmitted by simply staying in the OFF state (open circuit), and a 1 bit is transmitted by switching between both ON and OFF states (open circuit and 50 Ω) using a square-wave subcarrier frequency. Mathematically, the transmitted signal is written as

$$s_{\mathrm{rx}} = m \cdot \mathrm{sgn}\big(\sin(2\pi \mathrm{f_{sc}} t)\big), \qquad [3]$$

where m represents the bit to be encoded and takes on a 0 or 1 value. The subcarrier frequency is defined as f_{sc}.

Packet Detection and Demodulation. Our system assumes that the f_{sc} is known on the RX side, which allows us to perform heterodyne detection. Our demodulation is inspired by techniques used in radio astronomy, in particular, the Dicke radiometer (12). We can view our entire system as a distributed Dicke radiometer, where the switching between two states occurs on the TX side, while the amplification and integration occur on the RX side. The receiver performs heterodyne detection which allows the system to reject noise by filtering out any received signal power that is outside the narrow bandwidth of the subcarrier. In other words, the receiver generates the same square-wave subcarrier signal with amplitude values of +1 and −1, multiplies the received signal with this receive-side subcarrier, and accumulates (integrates) the product values for a duration that is less than or equal to that of the duration of one bit. This process results in a demodulated signal intensity and is given by,

$$\langle s_{\mathrm{rx}}, s_{\mathrm{sc}} \rangle = \int_0^T s_{\mathrm{rx}}(t) s_{\mathrm{sc}}(t) dt, \qquad [4]$$

where T is the total integration time. The demodulated signal intensity is compared to a threshold value to determine whether a 1 or 0 bit was transmitted. To successfully extract a data payload, data packets are transmitted that are structured to begin with a known preamble which is then followed by the data payload. The preamble is used to perform synchronization and then extract the data bits. In this implementation, a 7-bit Barker code is used. In Fig. 1*B*, we show an example of a received data packet before

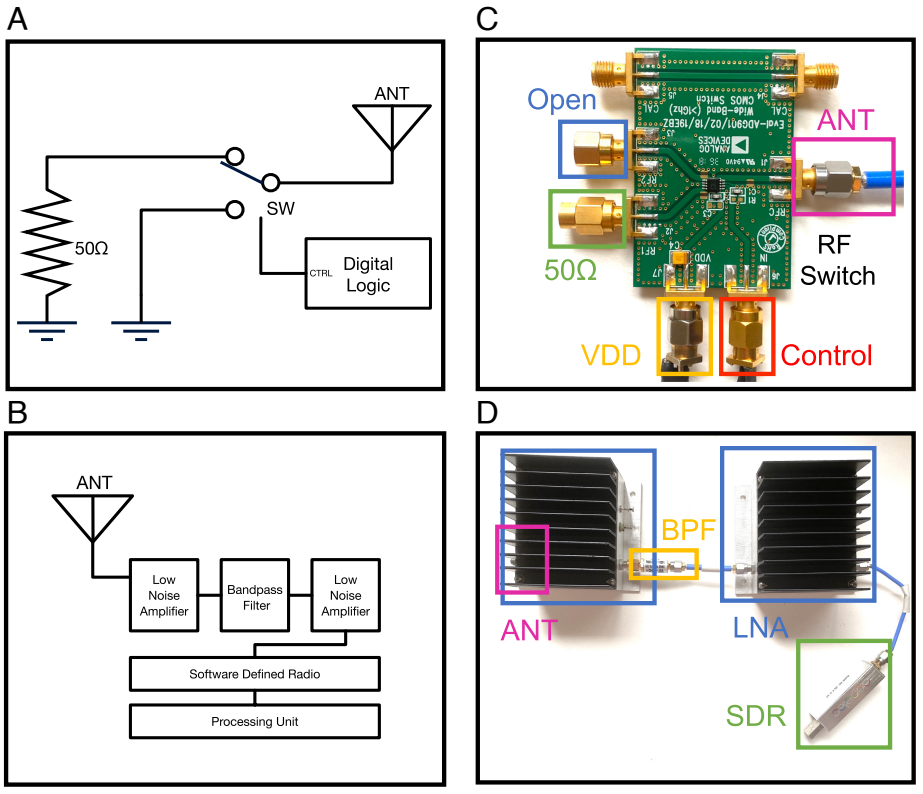

Fig. 2. Design and implementation. (*A*) shows the transmitter design, which switches between a 50-Ω load and short circuit (or open circuit) to modulated information bits. (*B*) shows the receiver, which is composed of two low noise amplifiers (LNA) whose output is fed into a software-defined radio. The bandpass filter between the two LNAs is added to prevent feedback oscillation, and the data received by the SDR can be processed by a laptop PC or small form factor computer (e.g., Raspberry Pi). (*C*) and (*D*) show the prototype implementation of the transmitter and receiver, respectively.

demodulation that was wirelessly transmitted, and in Fig. 1*C*, we show the data packet after demodulation and its binary format after performing thresholding.

System Validation

With this method of wireless communication comes two key questions that must first be answered: 1) Are we indeed modulating Johnson noise and not another source (e.g., ambient RF or control signal feedthrough)? and 2) How does modulated Johnson noise work if the entire system is at thermal equilibrium?

Evaluating Feedthrough. One concern that comes up with this system is whether there is feedthrough from the control signal used for the RF switch. We have performed control experiments to evaluate signal isolation. If the system is truly using thermal noise, then if it is configured to switch between two open circuit loads or two 50-Ω loads at room temperature, it should not be possible to decode data transmissions. We evaluate these two

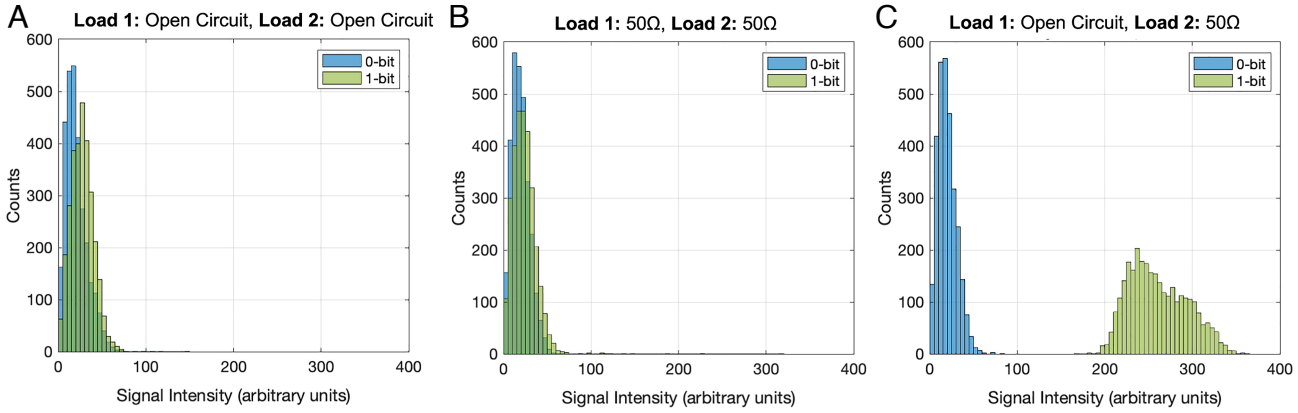

Fig. 3. Feedthrough evaluation. To ensure that the system has proper signal isolation, we evaluate the possibility of feedthrough from the control signal used for the RF switch in the transmitter. In (*A*), the histogram distribution of 0- and 1-bit transmissions after demodulation when switching between two identical open circuit loads is shown. Similarly, (*B*) shows the results when switching between two identical 50-Ω loads at room temperature. In (*A*) and (*B*), the 0 and 1 bits are not distinguishable. However, when switching between an open circuit and 50-Ω load, shown in (*C*), there is a clear difference between 0- and 1-bit transmissions.

scenarios and compare the results to that of switching between 50 Ω and an open circuit.

An additional potential concern is that we might not truly be using Johnson noise. Perhaps some preexisting RF signals, such as 60 Hz, broadcast TV, or even galactic emissions from neutral hydrogen, are being picked up in our apparatus and then being modulated by our two different load resistances, resulting in different outputs from our TX antenna. To control for this, we tested our data transmission method by switching between two 50-Ω loads at drastically different temperatures inside an anechoic chamber. If we truly are using Johnson noise, and not some other mechanism related to the different impedances, then two identical impedances at different temperatures should also work. We demonstrate that data can be modulated by switching between a 50-Ω load at room temperature (296 K) and a 50-Ω load submerged in liquid nitrogen (77 K).

(1) Control experiment: Feedthrough. A cabled benchtop experiment is set up to evaluate the three different scenarios. Data bits (1 and 0) are transmitted and then demodulated by the receiver. The demodulated data are presented in the form of histogram distributions which show the signal intensity of demodulated 1 and 0 bits. The open circuit and 50-Ω loads used were RF-shielded terminators. In Fig. 3*A*, we show the system evaluated when switching between two open circuit loads. In Fig. 3*B*, we show the system evaluated when switching between two 50-Ω loads. We compare this to the results shown in Fig. 3*C*, where the system is switching between open circuit and 50 Ω. From these results, we can see that when switching between two open circuit states or two 50-Ω states, the distribution of 1 and 0 bits look nearly identical. On the other hand, when switching between open circuit and 50 Ω, this is a clear difference between 1- and 0-bit transmissions.

(2) Control experiment: Temperature modulation. Using the same hardware setup as for the feedthrough experiments, we modulate information bits by switching between two 50-Ω loads that are at two different temperatures. A 50-Ω load is submerged in liquid nitrogen (77 K), while the other 50-Ω load is at room temperature (296 K). Using the cabled experimental setup, we transmit data packets by switching between the two states. In Fig. 4*A*, we show the distribution of 1 and 0 bits after demodulation, and in Fig. 4*B*, we show the demodulated data. Here, data are transmitted using a data rate of 5 bps and a subcarrier frequency of 100 Hz.

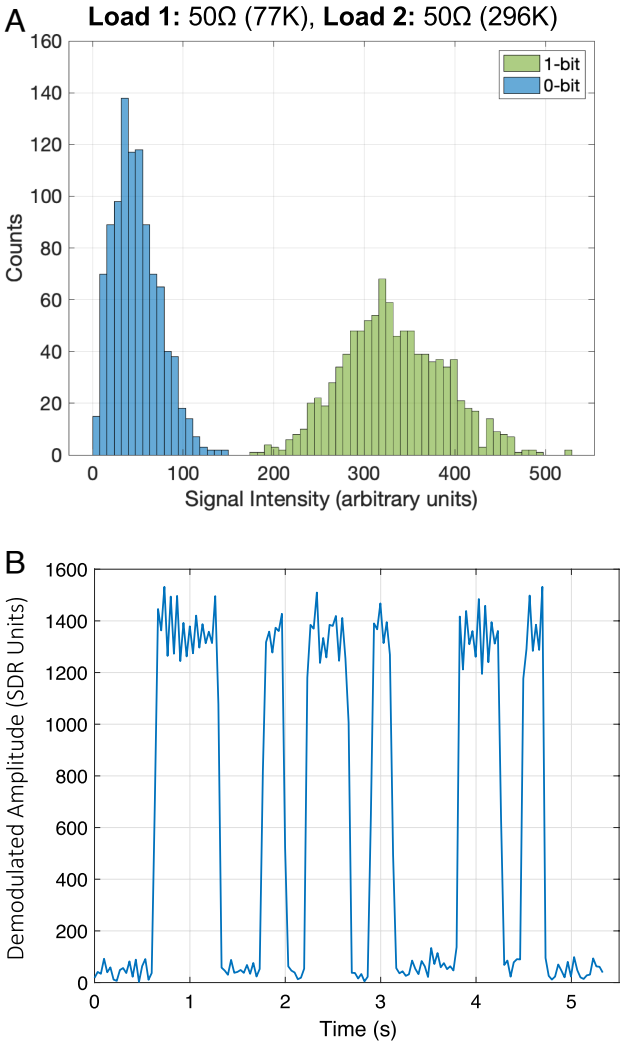

Fig. 4. Temperature modulation. Since Johnson noise power is a function of temperature, it should be possible to transmit information by switching between two 50-Ω loads that are at drastically different temperatures. We modulate information bits by switching between two 50-Ω loads, where one load has a temperature of 296 K, and the other has a temperature of 77 K. (*A*) shows the histogram distribution of 1 and 0 bits after demodulation, and (*B*) shows a demodulated data packet.

Evaluating Noise Temperature. One may worry that if the entire experiment is done at a single temperature (e.g., room temperature), then it should not be possible to observe modulated thermal signals due to a lack of contrast between the resistor and its surroundings. The question can be refined further: there are two separate potential issues. First, the transmit side and the receive side are at the same temperature, and second, the two loads on the transmit side (50 Ω and open circuit) are at the same temperature as one another. In the following sections, we address these concerns by first discussing the temperature contrast between TX and RX, as well as 50-Ω and open circuit loads. We then present experimental measurements that estimate the noise temperature of each load and compare the measured noise of each load to a theoretical analysis.

(1) TX-RX contrast. If the receive side and the transmit side of the system are at the same temperature, does this mean that our method should not work? If this was the case, then by the same argument, it would not be possible in a cabled experiment for our room temperature low noise amplifier to observe a change in Johnson noise power when we switch between a room temperature 50-Ω load and a room temperature open circuit. In fact, this is easily observed, as shown in Fig. 8*F*.

Active amplifiers, in particular, the LNA in our receiver, are not in thermal equilibrium and are characterized by a noise temperature (T_N) that is "cold," lower than the physical temperature (T_P) of the apparatus itself. This means that the radiation emitted by the receive antenna coupled to the LNA is equivalent to that of a colder 50-Ω resistor.

(2) 50-Ω open contrast. The two loads we switch between for signaling are at the same temperature. Furthermore, the Johnson noise power is independent of the value of the resistance. Thus, one might worry that no useful contrast can be generated. We analyze this quantitatively below, but it is significant that the 50-Ω load is well matched (to the LNA input in the cabled case and to the transmit antenna in the wireless case), and the open and short are poorly matched.

To evaluate this model quantitatively, we first measure the impedance of the open, short, and 50-Ω loads at our operating frequency of 1.42 GHz using a network analyzer. Fig. 5 shows the impedance of the open, short, and 50-Ω loads. As expected,

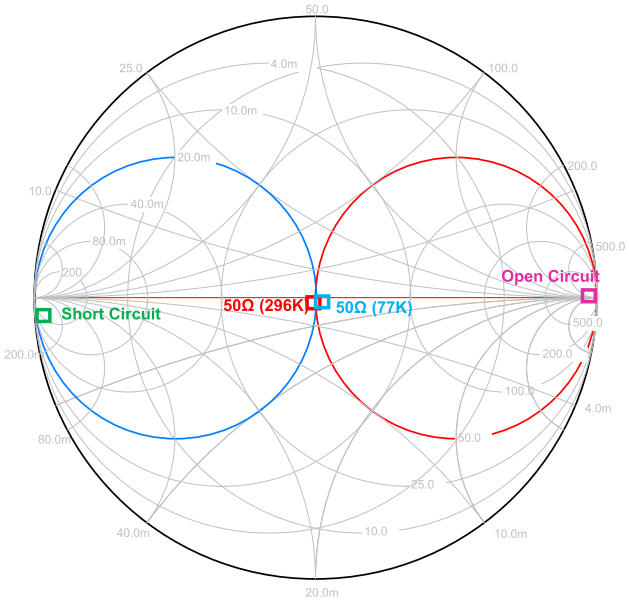

Fig. 5. Load impedance. A Smith chart showing the impedance of each evaluated load. The open and short circuits are both mismatched and have an impedance of approximately $Re(Z) = 17\ k\Omega$ and $Re(Z) = 0.25\ \Omega$, respectively. The 50-Ω load is very well matched and has a 50-Ω impedance at both 296 K and 77 K.

the open and short circuit are both mismatched and have a real impedance ($Re(Z)$) of approximately 17 kΩ and 0.25 Ω, respectively.

To predict the mean squared Johnson noise voltage across the load resistor, we plug these measured real impedance values into the expression for the mean squared Johnson noise voltage from Eq. **1**. Now, we need to model the effect of the LNA, in particular, the effect of its input impedance on the measured signal. The input impedance of the LNA is 50 Ω, meaning that it can be modeled as an equivalent circuit with a 50-Ω resistor to ground and an infinite input impedance amplifier observing the voltage at the junction between the LNA's input and this 50-Ω shunt resistor (13). (We could use a more complete model that includes the noise of the amplifier, but this is not essential for our purposes in the present discussion.) Fig. 6 shows the voltage divider formed by the noise source and R_2; the voltage at the junction of R_1 and R_2 is observed by the LNA. The mean squared voltage observed by the amplifier, $\langle V^2 \rangle$, is given by

$$\langle V^2 \rangle = \langle V_f^2 \rangle \cdot g^2 = 4kTBR_1 \cdot g^2, \quad [5]$$

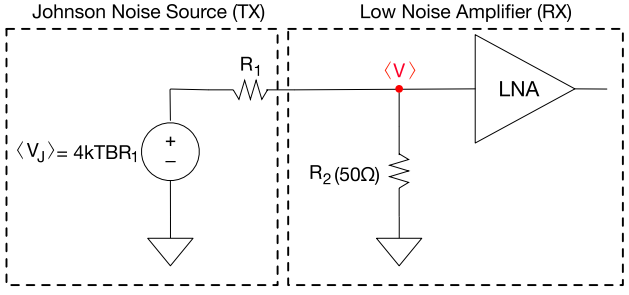

Fig. 6. Equivalent circuit. The equivalent circuit model for a cabled scenario showing the voltage divider formed by a noisy resistor and LNA input impedance.

where

$$g = \frac{R_2}{R_1 + R_2}, \quad [6]$$

is the gain of the voltage divider. As shown in Fig. 5, R_1 is a noiseless resistor and represents the resistance of the Johnson noise source, and R_2 = 50 Ω is the LNA's input impedance. The infinite input impedance amplifier block in Fig. 6 measures the voltage V at the node where R_1 and R_2 connect. The mean squared input voltage to the amplifier is given by Eq. **5**. Expressed as multiples of kTB, the mean squared noise voltages $\langle V^2 \rangle$ for our open, short, and 50-Ω loads are predicted to be

$$\langle \mathrm{V}^2_{\mathrm{open}} \rangle = 0.58 \cdot kTB,$$

$$\langle \mathrm{V}^2_{\mathrm{short}} \rangle = 1.0 \cdot kTB,$$

$$\langle \mathrm{V}^2_{50} \rangle = 50 \cdot kTB.$$

The varying constants in front of kTB demonstrate that the impedance matching differences lead to small signals from the open and short and larger signals from the 50-Ω load. Later (after addressing calibration), we provide a detailed comparison of predicted mean squared noise voltages to experimentally measured values for each of the loads of interest, shown in Table 1. Note that the experimentally observed contrast between the loads is less than the theoretical differences here because of degradation in signal-to-noise ratio (SNR) caused by noise added by the receive signal chain, which we neglected in this discussion.

(3) Experimental measurements and calibration overview. We measure the noise produced by each load of interest in a cabled benchtop experiment and use this to compute the corresponding noise temperature along with calibration parameters (i.e., receiver noise offset and gain). In addition to measuring the noise of the 50-Ω load at room temperature, we also evaluate the 50-Ω load when submerged in ice water (273 K) and liquid nitrogen (77 K). The three different temperatures for the 50-Ω load are considered to be *known* temperatures. One special load of interest we evaluate in addition to the communication loads is an LNA input, in order to characterize its effective temperature.

We collected 60 million measurements of the noise generated by each of the loads and found for each the mean squared voltage $\langle \widehat{V}^2_{s_{rx}} \rangle$ using

$$\langle \widehat{V}^2_{s_{rx}} \rangle = \frac{1}{N} \sum {s_{rx}}^2, \quad [7]$$

where s_{rx} is the received signal.* The hat (such as in $\widehat{V}_{s_{rx}}$) indicates that the voltages are in arbitrary SDR units. Voltages without a hat are in physical units (Volts). Using measurements of the 50-Ω load at the three known temperatures, we performed a linear fit of $\langle \widehat{V}^2_{s_{rx}} \rangle$ versus temperature. Using this linear fit, we extracted the noise temperature of the remaining loads (LNA Input, open, and short) from the observations of $\widehat{V}_{s_{rx}}$. Fig. 7 shows the results, which indicate that the LNA's noise temperature is cold (39 K), much colder than a 50-Ω load at room temperature (296 K). The open and short circuit loads also appear colder than room temperature. The short circuit terminator has a physical temperature of 296 K, but its noise temperature is 46 K. The open circuit has a noise temperature of 40 K.

*In particular, it is the real part of the complex values provided by the SDR; the imaginary part has the same statistics.

Table 1. Computing theoretical Gaussian distribution

Load	T_P (K)	T_N (K)	G_{RX}	B (Hz)	Offset	$\widehat{V}^2$ predicted from measured T_P	$\widehat{V}^2$ calculated from extracted T_N	$\widehat{V}^2$ measured
50 Ω (room temperature)	296	296				0.0676	–	0.0676
50 Ω (liquid nitrogen)	77	77				0.0332	–	0.0333
Open circuit	296	46	2.3e11	1e6	0.0212	0.0217	–	0.0274
Short circuit	296	40				0.0221	–	0.0283
LNA input	–	39.5				–	0.0274	0.0273

This table shows the parameters used to compute the theoretical $\widehat{V}^2$ for each load. The theoretical $\widehat{V}^2$ values can be compared with the measured $\widehat{V}^2$ in the last column of the table. In the theoretical Gaussian distributions later in the paper, the variable $\widehat{V}^2$ from this table is renamed σ^2. The T_P values above are measured physical temperatures. The T_N values for the 50-Ω loads are assumed, to produce the linear calibration curve shown in Fig. 7. The other T_N values in the column are extracted by applying this linear calibration curve to the measured $\widehat{V}^2$ values.

(4) Comparing theoretical and observed noise distributions. To compare our experimental measurements with expected theoretical values, we also need to perform some calibration. In particular, we need to find the baseline or offset noise produced by the receive chain as well as the gain value that converts between the SDR's arbitrary units and volts. This calibration of arbitrary SDR units to volts will allow us to compare the theory and experiment for the less obvious loads, namely the open and the short. Using our results from Fig. 7, we know that the receive chain introduces noise equivalent to an offset of 0.0212 in arbitrary SDR units. In other words, the offset is the $\langle \widehat{V}^2_{s_{rx}} \rangle$ value at the y-intercept of the linear fit. The gain, which is constant across all measurements, can be computed by determining the ratio of the measured data for any particular load to the expected theoretical value and then using this same value for all other datasets. The gain is given by,

$$G_{\mathrm{RX}} = \frac{\langle \widehat{V}^2_{s_{rx}} \rangle - offset}{\langle V^2 \rangle}. \qquad [8]$$

Now, we can compare our theoretical model (based on impedance mismatch of Johnson noise) to measured values. For each load, we compare the histogram of our observed noise measurements with the theoretical distribution.

To find the distributions, recall that Eq. **5** predicts $\langle V^2 \rangle$ as a function of temperature, bandwidth, Johnson resistor value, and LNA input impedance. Since thermal noise is white, the distribution of the real or imaginary voltages is Gaussian with $\mu = 0$ and $\sigma = \sqrt{\langle V^2 \rangle} = V_{RMS}$. We know from the results in Fig. 5 that $R_1(short) = 0.254\,\Omega$ and $R_1(open) = 17\,k\Omega$ at our frequency of interest. We also must account for the gain and offset of the receive chain. As previously mentioned, the receive chain introduces noise equivalent to an offset of 0.0212 in arbitrary SDR units. We can also compute the receiver gain using Eq. **8**. Now, the variance σ^2 (which we also refer to as $\langle \widehat{V}^2_{s_{rx}} \rangle$) can be related to the theoretical value of $\langle V^2 \rangle$ using

$$\sigma^2 = \langle V^2 \rangle \cdot G_{\mathrm{RX}} + offset. \qquad [9]$$

The Gaussian distribution is then computed for each case:

$$f(x) = \frac{1}{\sqrt{2\pi}\sqrt{\sigma^2}} \cdot e^{-\frac{1}{2}\left(\frac{x-\mu}{\sqrt{\sigma^2}}\right)^2}. \qquad [10]$$

Fig. 8 shows the histogram distribution of the measured data for each load and the corresponding theoretical distribution. The bandwidth is determined by the bandwidth of the SDR, and, in particular, its antialiasing filters.

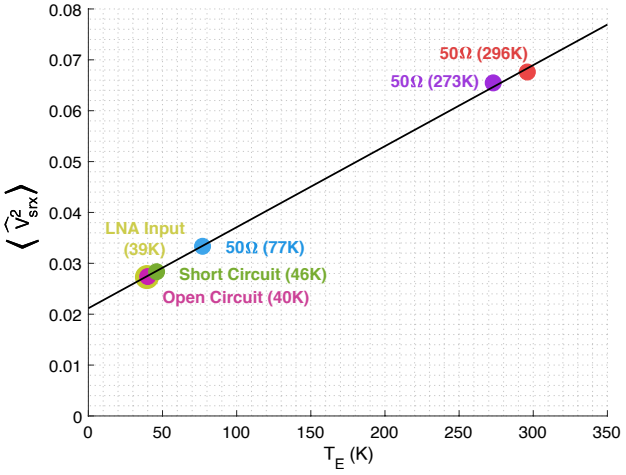

Fig. 7. Noise temperature. The measured mean square noise voltage and noise temperature for each load. The three 50-Ω loads at known temperatures were used to calibrate the noise temperatures for the other loads. Here, the linear fit equation is $\langle \hat{V}^2_{srx} \rangle = 0.000159 \cdot T + 0.0212$

Performance

The performance of the wireless communication system is evaluated in terms of achievable throughput and communication range by conducting wireless experiments using the previously described hardware. Additionally, we demonstrate the potential for battery-free sensing by implementing a battery-free transmitter that transmits data by modulating Johnson noise.

Achievable Throughput. To evaluate achievable throughput, the measurements were performed inside of an anechoic chamber. This allows us to test the system in an interference free environment and to achieve best possible performance given our hardware implementation and the modulation and demodulation scheme. Measurements were taken every 1.5 m and up to 4.5 m inside the anechoic chamber, and at each distance, data packets were transmitted wirelessly. The data packet structure includes a 7-bit Barker code as the preamble, followed by a 13-bit data payload. At each distance, the maximum achievable throughput was determined by measuring which data rate would allow us to achieve a bit-error-rate (BER) less than or equal to 1%. Fig. 9*A* shows that the maximum achievable throughput is 26 bps at 1.5 m and goes down to 22 bps at 4.5 m. Moreover, the number of samples per bit was fixed to 5 while the subcarrier frequency was varied, which in turn varies the data rate. For example, at 2.3 m, the achievable throughput was 26 bps, and data were

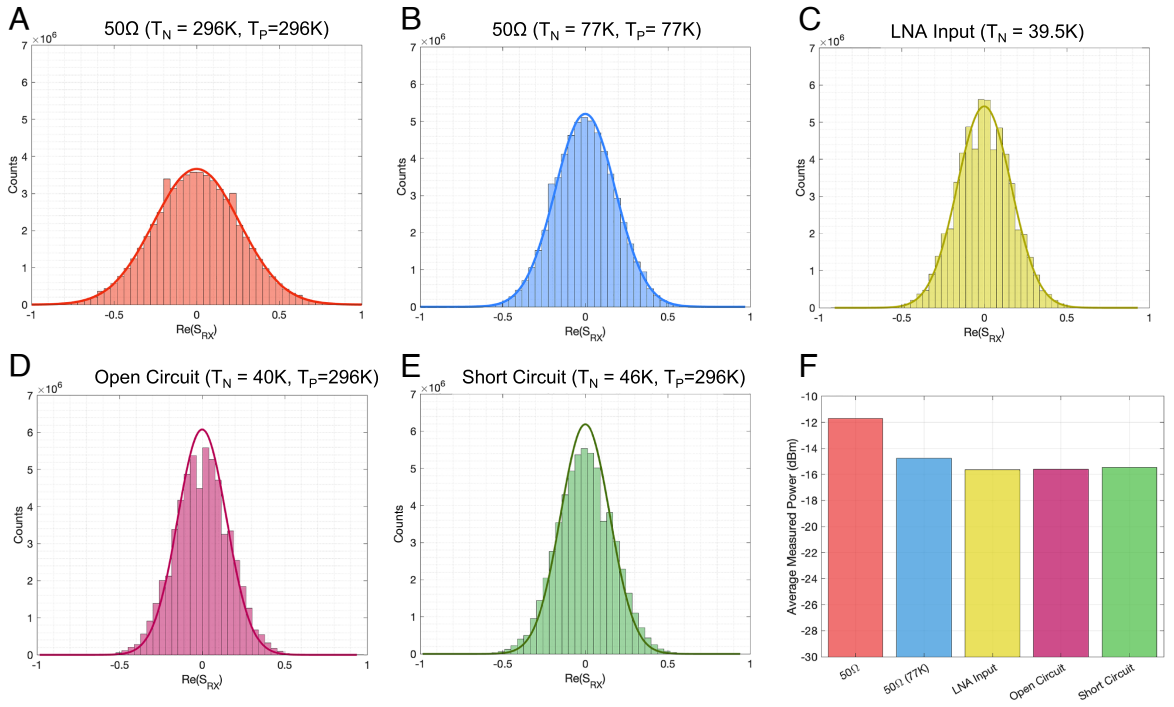

Fig. 8. Theoretical noise distributions compared to data. For each load, the noise temperature T_N and physical temperature T_P are indicated at the top of the plot. (*A*) Histogram distribution of the real component of the measured data for the 50-Ω terminator at room temperature (296 K). The theoretical Gaussian distribution is overlaid on the data. (*B*) 50-Ω terminator in liquid nitrogen (77 K). (*C*) The LNA input has a noise temperature T_N = 39 K. Its low temperature is important to the operation of the system. (*D*) The short circuit terminator has a low effective temperature T_N = 46 K because it is poorly matched to the LNA. (*E*) The open circuit terminator has a low temperature of T_N = 40 K, also because of mismatch. (*F*) A comparison of the average measured power of each load in dBm after amplification.

modulated by using a 130-Hz subcarrier frequency. At 4.6 m, the achievable throughput was 22 bps, and data were modulated by using a 110-Hz subcarrier frequency.

Communication Range. The wireless communication range is evaluated in an outdoor environment, as shown in Fig. 9*C*. Here, measurements were taken starting from 1.8 m and up to 7.3 m

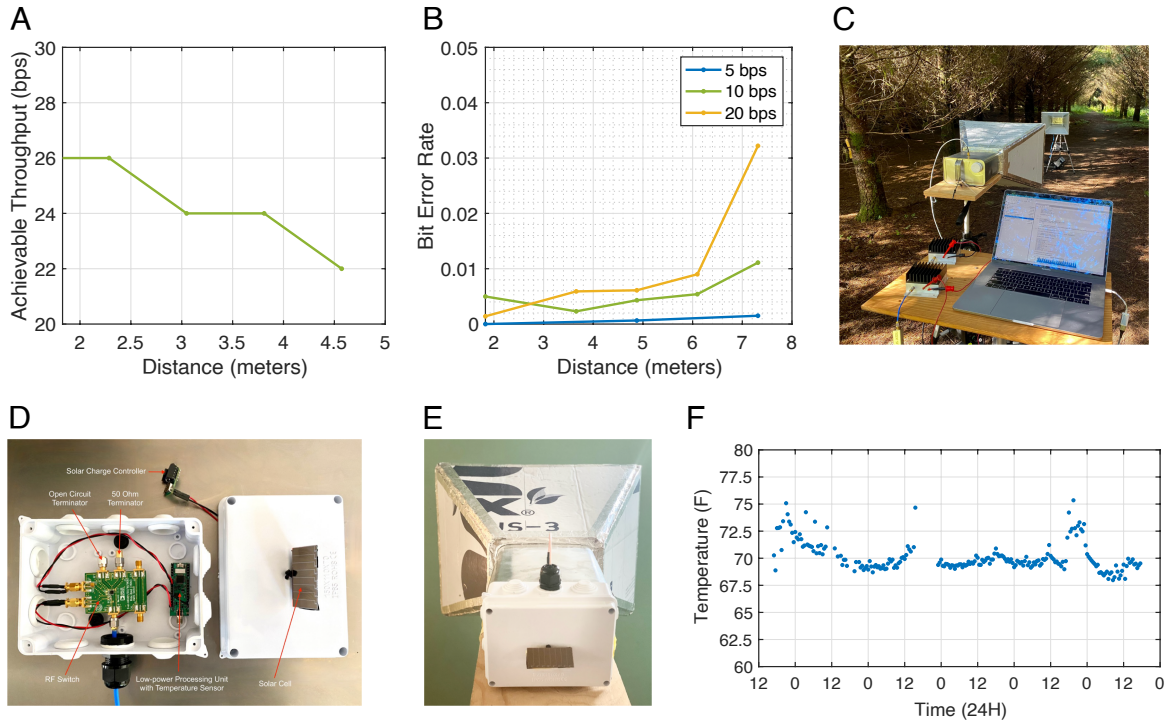

Fig. 9. Performance evaluation. (*A*) shows the achievable throughput with respect to distance, which was evaluated wirelessly inside an anechoic chamber. (*B*) shows the bit-error-rate with respect to distance for three different data rates: 5 bps, 10 bps, and 20 bps. Here, the communication range was evaluated wirelessly in an outdoor setting as shown in (*C*). (*D*) and (*E*) show a battery-free transmitter prototype that collects ambient temperature data and transmits the information by means of modulated Johnson noise. The temperature plot in (*F*) shows the data that were collected wirelessly across five consecutive days in a residential building.

for three different data rates. We evaluate the communication range using data rates of 5, 10, and 20 bps. Fig. 9*B* shows the range performance results. As expected, a higher data rate results in a short communication range. For example, with a data rate of 20 bps, the maximum communication range is approximately 6.1 m, whereas using a data rate of 5 bps, the communication range increases to approximately 7.3 m while having a BER = 0.15%.

Solar-Powered Battery-Free Transmitter. We demonstrate the potential for battery-free sensing using modulated Johnson noise, by developing a solar-powered battery-free transmitter, as shown in Fig. 9 *D* and *E*. The transmitter includes an ADG901 RF switch and a custom PCB that integrates a low-power microcontroller (MCU), temperature sensor, and solar energy harvester (14). The custom printed circuit board (PCB) is used to collect temperature data, packetize the data, and control the RF switch to modulate data. The transmitter is powered using a small 2.54-cm × 6.35-cm solar cell that charges a supercapacitor instead of relying on a battery. We deploy the transmitter inside a residential building to monitor ambient temperature data and transmit the information by means of modulated Johnson noise. The data were received using the receiver hardware previously described. In Fig. 9*F*, we show the temperature collected across five days. Note that no error-correcting codes were implemented, which resulted in some anomalies in the ambient temperature data collection.

Conclusion

This paper opens up a direction for low-power wireless communication by demonstrating that information bits can be wirelessly transmitted by modulating Johnson noise. By selectively connecting and disconnecting an impedance-matched resistor to an antenna, data can be wirelessly transmitted with no active oscillator on either the transmit or the receive side and no preexisting RF carrier, as in backscatter and ambient backscatter communication. We have demonstrated that our system can achieve data rates up to 26 bps and a communication range as far as 7.3 m. This method has many attractive features compared to previous passive communication schemes such as ambient backscatter or RFID because it is not reliant on ambient or generated RF sources. One of the challenges faced by backscatter communication is the increased system complexity: Conventional half-duplex radio transmission requires just two entities, a transmitter and a receiver. Backscatter requires three entities because it needs a carrier generator in addition to the data transmitter and receiver. (In a monostatic backscatter reader, the carrier generator is packaged with the receiver, but the system architecture is still more complex.) In addition to the deployment benefits of the simplified system architecture, the absence of a carrier means that the reader device does not need to contend with self-jamming caused by the carrier, which is a key driver of RFID reader complexity and cost. While the performance of the prototype system is modest, we hope that the techniques presented will lead to an avenue of research and help realize the vision of ubiquitous computing.

Data, Materials, and Software Availability. All study data are included in the article and/or *SI Appendix*.

ACKNOWLEDGMENTS. We thank A. Saffari and D. Nissanka for assisting in the prototype development, S. Garman for performing antenna characterization, and M. Reynolds for suggesting the experiment with two 50-Ω resistors at different temperatures. The work was funded by NSF CNS-1823148 and a Microsoft Research Dissertation Grant.

1. H. Stockman, Communication by means of reflected power. *Proc. IRE* **36**, 1196–1204 (1948).
2. V. Liu *et al*., Ambient backscatter: Wireless communication out of thin air. *SIGCOMM Comput. Commun. Rev.* **43**, 39–50 (2013).
3. L. B. Kish, Stealth communication: Zero-power classical communication, zero-quantum quantum communication and environmental-noise communication. *Appl. Phy. Lett.* **87**, 234109 (2005).
4. J. Qu *et al*., Johnson noise thermometry. *Meas. Sci. Technol.* **30**, 112001 (2019).
5. J. B. Johnson, Thermal agitation of electricity in conductors. *Phys. Rev.* **32**, 97–109 (1928).
6. H. Nyquist, Thermal agitation of electric charge in conductors. *Phys. Rev.* **32**, 110–113 (1928).
7. D. M. Pozar, *Microwave Engineering* (John Wiley & Sons, Inc., 2012).
8. Analog, Evaluation board for the ADG901/ADG902 (2022). https://www.analog.com/media/en/technical-documentation/user-guides/EVAL-ADG901EBZ902EBZ918EBZ919EBZ.pdf.
9. MiniCircuits, ZHL-1217HLN+ low noise amplifier (2022). https://www.minicircuits.com/pdfs/ZHL-1217HLN+.pdf.
10. NooElec, NESDR SMArt XTR (2022). https://www.nooelec.com/store/sdr/sdr-receivers/nesdr-smart-xtr.html.
11. MiniCircuits, VBF-1445+ bandpass filter (2022). https://www.minicircuits.com/pdfs/VBF-1445+.pdf.
12. D. F. Wait, The sensitivity of the dicke radiometer. *J. Res. Nat. Bur. Stand. C* **71**, 127–152 (1967).
13. J. Denker, Perspectives on Johnson noise (2015). https://www.av8n.com/physics/johnson-noise.htm.
14. M. Katanbaf, A. Saffari, J. R. Smith, "Multiscatter: Multistatic backscatter networking for battery-free sensors" in *Proceedings of the 19th ACM Conference on Embedded Networked Sensor Systems, SenSys 2021* (Association for Computing Machinery, New York, NY, USA, 2021), pp. 69–83.